Volume 12, Issue 3, Page 118-127, 2023 https://doi.org/10.46810/tdfd.1324471 Research Article

BİNGÖL ÜNİVERSİTESİ

Türk Doğa ve Fen Dergisi
Turkish Journal of Nature and Science
www.dergipark.gov.tr/tdfd

The Effect of Alumina Additive on the Properties of Sheep Hydroxyapatite

Süleyman Serdar PAZARLIOĞLU[1*]

[1] Marmara University, Technology Faculty, Metallurgy and Materials Science and Engineering Department, İstanbul, Türkiye
Süleyman Serdar PAZARLIOĞLU ORCID No: 0000-0002-7870-8418

**Corresponding author: spazarlioglu@marmara.edu.tr*

(Received: 08.07.2023, Accepted: 11.09.2023, Online Publication: 27.09.2023)

Keywords
Sheep hydroxyapatite, Alumina, Sintering, Property

Abstract: In this study, the effect of alumina (Al_2O_3) addition, varying between 1-10% by weight, on the properties of hydroxyapatite obtained from sheep femur bones (SHA) was investigated. SHA decomposed at all sintering temperatures and the total decomposition rate increased from 1.4% to 4.1% with increasing temperature. The decomposition rate of SHAs with Al_2O_3 added increased to 60.1% with increasing Al_2O_3 and sintering temperature. Density (from 2.16±0.03 to 2.98±0.02 g/cm^3) and hardness (from 0.93±0.15 GPa to 3.90±0.27 GPa) of SHA increased with increasing temperatures, however; the highest compression strength (82±5.05 MPa) and fracture toughness (0.70±0.11 MPam$^{1/2}$) were obtained at a temperature of 1200ºC. Additions at amount of 1% and 2.5% Al_2O_3 to SHA contributed to obtaining better properties than 5% and 10%, however; the optimum Al_2O_3 ratio is 2.5% and the sintering temperature is 1200ºC. With the addition of Al_2O_3 at amount of 2.5%, the fracture toughness value of SHA increased from 0.70±0.11 MPam$^{1/2}$ to 1.70±0.15 MPam$^{1/2}$, and the compression strength increased from 82±5.05 MPa to 207.85±5.85 MPa. The brittleness index of SHA increased from 1.70±0.27 to 7.10±0.50 $\mu^{-1/2}$ with increasing temperature. It increased to 3.56±0.18 $\mu^{-1/2}$ as the maximum value by the addition of Al_2O_3 to SHA. At the end of the 28-day immersion period, it was determined that, most of the SHA surface and the entire surface of the SHA-2.5Al_2O_3 composite were covered with apatite layer.

Alumina İlavesinin Koyun Hidroksiapatitin Özelliklerine Etkisi

Anahtar Kelimeler
Koyun hidroksiapatit, Alumina, Sinterleme, Özellik

Öz: Bu çalışmada ağırlıkça %1-10 arasında değişmekte olan alumina (Al_2O_3) ilavesinin koyun femur kemiklerinden elde edilmiş olan hidroksiapatitin (SHA) özelliklerine etkisi incelenmiştir. SHA tüm sinterleme sıcaklıklarında dekompoze olmuş ve toplam dekompoze olma oranı artan sıcaklıkla %1.4' ten %4.1' e çıkmıştır. Al_2O_3 ilaveli SHA' lerde dekompoze olma oranı ise artan Al_2O_3 ve sinterleme sıcaklığı ile %60.1' e artmıştır. SHA' nın yoğunluğu (2,16±0,03' ten 2,98±0,02 g/cm^3' e) ve sertliği (0,93±0,15 GPa' dan 3,90±0,27 GPa' ya) artan sıcaklık arttıkça artmış, ancak; en yüksek basma dayanımı (82±5,05 MPa) ve kırılma tokluğu (0,70±0,11 MPam$^{1/2}$) 1200ºC sıcaklıkta elde edilmiştir. SHA' ya %1 ve %2.5 oranında Al_2O_3 ilavesi, %5 ve %10' dan daha iyi özelliklerin elde edilmesine katkı sağladı; optimum Al_2O_3 oranı %2.5 ve sinterleme sıcaklığı 1200ºC' dır. %2.5 oranında Al_2O_3 ilavesi ile SHA' nın kırılma tokluğu değeri 0,70±0,11 MPam$^{1/2}$' den 1,70±0,15 MPam$^{1/2}$' ye, basma dayanımı 82.48±5.05 MPa' dan 207.85±5.85 MPa' ya yükselmiştir. SHA' nın kırılganlık indeksi artan sıcaklıkla 1.70±0.27'den 7.10±0.50 $\mu^{-1/2}$'ye yükseldi. SHA' ya Al_2O_3 ilavesiyle maksimum değer olarak 3,56±0,18 $\mu^{-1/2}$' ye yükseldi. 28 günlük daldırma süresi sonunda SHA yüzeyinin büyük bir kısmının, SHA-2.5Al_2O_3 kompozitinin yüzeyinin ise tamamının apatit tabakası ile kaplandığı belirlendi.

1. INTRODUCTION

Waste mineralized tissues (WMT) create an undesirable environmental impact [1]. The most effective method for minimize the environmental impact of WMT is to transform their into useful and valuable substances through ecofriendly processes [2]. WMT, such as bone, teeth, antler and horn, are important elemental storage

sites in animals. These tissues contain necessary elements, both major, such as calcium (Ca), phosphorus (P), magnesium (Mg) and sulphur (S), and trace elements, such as iron (Fe), zinc (Zn), manganese (Mn) and cadmium (Cd). [3]. These ingredients serve as catalytic, structural, and electrochemical components in numerous applications. Furthermore, bones are utilized in food and biomedical sector due to their rich component. Waste bone derived hydroxyapatite (HA) has further usage in drug delivery agents, adsorbents, chemical sensors, bio-ceramics, chromatographic lighting materials, and powder carriers [4]. Waste bone of animals such as chicken [5], turkey [6], bovine [7], goat [8], and pork [9] can be used in the production of HA. Sheep bones are also suitable for medical research [10], because they have similar macrostructure to human bone [11]. Sheep bones can be also used as HA production resource [12]. HA is one of the non-toxic bioceramics that has biocompatibility and similarity in composition with human bones. Besides having advantages, HA has poor mechanical properties such as low values of hardness and fracture toughness and is brittle [13]. It has been stated by Demirkol, N., et al.[14] that SHA has the sintered density of 2.59 g/cm^3, the hardness of 189 HV and the compression strength of 69 MPa. These values restrict the use of SHA in the human body. The weak characteristic properties of SHA could be improved when it was reinforced with a material, which has higher mechanical reability than that of SHA [15]. Many studies have demonstrated that the addition of ceramics to SHA tends to enhance its mechanical performance and/or its biological properties [16]. For this purpose some ceramics such as niobium oxide [17], magnesium oxide [18], perlite [19] and bioactive glass [20] were used as reinforcement agent.

Alumina (Al_2O_3) is an advanced ceramics industry because of three key advantages: (i) it has an industrially high usable combination of mechanical, tribological, dielectric properties and chemical inertness; (ii) It is an inexpensive and easily available material [21]. Moreover, it has excellent properties, such as low thermal expansion coefficient, high chemical stability, and good high-temperature performance [22]. It has been declared that Al_2O_3 additive contributes the improvement of properties of dental [23] and femoral head of hip joint replacement materials [24]. Although Al_2O_3 has been used as a reinforcement agent for synthetic [25-27] and/or biologically derived HAs [28,29], its effect on SHA has not been investigated.

In the present study, the effect of alumina additive on the sinterability and properties of sheep derived hydroxyapatite was investigated using microstructural characterization techniques and mechanical testings.

2. MATERIAL AND METHOD

In the present study, hydroxyapatite was derived from sheep femur bones as shown in Figure 1. Sheep femur bones purchased from Migros (Kadıköy, Istanbul) were firstly cleaned to remove visible substances and then head parts of the bones were cut off and marrow in shafts removed via boiling within water in a pressure cooker for 4 h. After the boiling process, the retained shafts were deproteinized with sodium hidroxide (NaOH) for 1 h, washed with distilled water and then dried at 105ºC for 4h. before calcination treatment. Finally bones were calcinated at 800ºC for 2 h and then obtaining of HA was checked by XRD analysis. It is in good agreement with the ICDD Card No: 98-009-0247 for HA. The calcinated samples were firstly ground and then crushed in a mortar to between -63 µm to +45 µm to prepare the composites as shown in Figure 2.

Figure 1. Schematic presentation of the production of SHA powder

Figure 2 shows the processing steps of production of SHA with and without Al_2O_3 additives. Four different composites were prepared by adding Al_2O_3 to SHA, at amount of 1wt%, 2.5wt%, 5wt% and 10wt% , respectively. The prepared mixtures were homogenized with zirconia balls and ethyl alcohol at 180 rpm for 2 hours, with a powder/ball ratio of 1/7. SHA and composite powders were pelleted in accordance with British standard 7253 [30] using zinc stearate, and then dried at 105ºC. The green bodies were heated up to 300ºC to remove zinc stearate and sintered at the temperatures of 1100, 1150, 1200, 1250 and 1300ºC for 4 h.

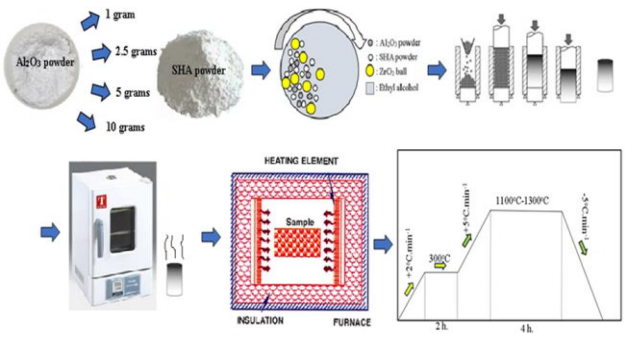

Figure 2 Processing steps of production of SHA with and without Al_2O_3 additive

Density, porosity and relative densities of the sintered samples were measured using a Precisa XB 320 M precision balance according to the Archimedes principle. The theoretical density of SHA was taken as 3.156 g.cm^{-3} [31] and the theoretical density of Al_2O_3 was taken as 3.970 g.cm-3 [32] to calculate the relative density of samples. Hardness of the samples were determined in the Future Tech FM301 device by using the Vickers ($HV_{0.2}$) method because it provided the formation of hardness indent without cracking. The sintered samples were ground with SiC papers (between 800 and 5000 mesh) and then polished with diamond paste up to 0.5 µ to obtain

mirror-like surfaces. Fracture toughness measurements were performed under a load of 2,943 N with a dwell time of 10 s and calculated according to Equation 1 [33].

$$K_{Ic} = 0.203(c/a)^{-1.5}(H_V)(a)^{0.5} \quad \text{(E1)}$$

Here; K_{IC} is the fracture toughness (MPa.m$^{1/2}$), c is the radial crack dimension measured from the center of the indent impression (m), H_V is the hardness (MPa), and a is the half diagonal of the indentation (m). The brittleness index of the sintered samples was calculated by Equation 2 [34].

$$BI = (HV/K_{Ic}) \quad \text{(E2)}$$

Here; B is brittleness index, HV is the hardness, and K_{Ic} is the fracture toughness.

Compression strength of the sintered samples was calculated by Devotrans FU 50kN testing device under a loading rate of 2 mm.min^{-1}. The surface morphology and grain size measurements of the samples were performed using the FEI Sirion XL30 scanning electron microscope (SEM). The phases in the SHAs with and without Al_2O_3 additive were analyzed using a Philips X'Pert X-ray diffraction (XRD, Netherlands) device in the range of 2θ values between 20° and 50°. Rietvield analysis was performed to calculate the phase ratios in the samples.

3. RESULTS & DISCUSSION

Figure 3 shows the XRD analysis of the pure SHA depending on the sintering temperature. It is seen that β, α-TCP and CaO phases are formed when pure SHA is sintered at 1300ºC. The same regime had also confirmed in a previous study [35]. Thermal stability of biologically derived HAs depends on a number of factors, such as Ca/P ratio of HA [36], calcination temperature and time [37] and sintering atmosphere [38], cause its decomposition [39]. Thermal stability of synthetic HA is around 1100-1150ºC; above this temperature, it is possible to see phase transformations [40]. Bovine HA has been reported to decompose into β-TCP at approximately 1100°C [41]. The termal decomposition of HA is attributed to the vacancies formed by release of structural water [42], and it can be explained as shown in Reaction 1 [38] when sintering is performed at 1300ºC.

$$Ca_{10}(PO_4)_6(OH)_2 \longrightarrow 3Ca_3(PO_4)_2 + Ca_3P_2O_8 + CaO + H_2O \quad \text{(R.1)}$$

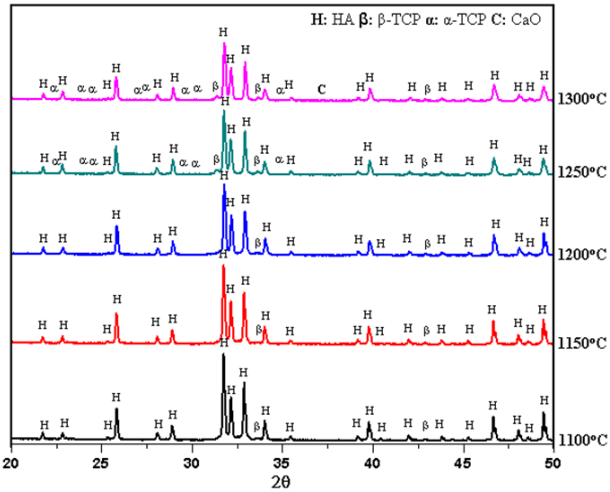

Figure 3. XRD analysis of the pure SHA depending on the sintering temperature.

A study mentioned that HA at the sintering treatment of 1200°C has occurred with β-TCP [43]. Breaking of the bond between the calcium ion and the hydroxyl ion leads to removal of the hydroxyl ion from the crystal, and HA eventually decompose to generate β-TCP [44]. The formation of OH^- vacancies accelerates the cation transport in the HA lattice and it increase the decomposition ratio of HA matrix material [45]. As shown in Table 1, the decomposition ratio of 1.4% of SHA at 1100ºC increased with ascent of sintering temperature and it was calculated as 4.1% at the sintering temperature of 1300ºC. It was declared by Lim, et al. [46] that the decomposition ratio of HA had 56% at the same temperature. However, a material produced to the human body applications should have a decomposition ratio lower than that of 10% according to ISO 13779-3:2018 standart [47]. There are several reasons for such a restriction: β-TCP existing in HA with low content helps for the rapid bonding of artificial bones to natural ones via rapid dissolution. Biphasic HA/β-TCP structures are being considered for filling periodontal osseous defects. The presence of a more bioactive phase (β-TCP) in the biphasic composite promotes a much faster osseointegration without complete implant resorption [48]. Too high content of β-TCP seriously deteriorates the mechanical properties and chemical stability of artificial bones. Thus, the precise control of β-TCP content in HAp is a critical issue in biomedical applications [49]. More than 10% of α-TCP in the HA matrix causes an increase in the number of nanopores, which severely reduces the strength of the sintered samples [50]. Moreover, the formation of a very high amount of highly soluble phase in HA ceramics, i.e. α-TCP, reduces the formation of an apatite-like layer in HA ceramics [51]. The presence of CaO in HA-based implants designed for medical applications is unacceptable for the following reasons. In contact with water molecules CaO converts into calcium hydroxide. That results in gradual tension and hair cracks in the ceramic material, its swelling and breaking and even some disintegration into individual particles and also generates strong alcalinity in the implant environment. The problem of the presence of CaO in the HA of animal origin is significant in respect of its applications as biomaterial [52].

Table 1 Rietveld analysis of pure SHA depending on the sintering temperatures

Temperature (°C)	Chemical composition (%)				Total decomposition ratio (%)
	HA	β-TCP	α-TCP	CaO	
1100	98.6	1.4	-	-	1.4
1150	98.0	2.0	-	-	2.0
1200	97.8	2.2	-	-	2.2
1250	97.4	1.0	1.6	-	2.6
1300	95.9	1.3	2.6	0.2	4.1

XRD patterns of Al_2O_3 added SHAs are presented in Figure 4. For the SHA/1Al_2O_3 composite, HA decomposed to β-TCP at 1100°C; and at 1200°C HA started to decompose the mixture of β- and α-TCP. After sintering at 1300°C, 5.0% of the HA tranformed into β-TCP and 3.0% of the HA tranformed into α-TCP in this composite as shown in Table 2. In the composites of SHA/2.5Al_2O_3 and SHA/5Al_2O_3, HA transformed to β-TCP. A transformation at about 8.1% for SHA/2.5Al_2O_3, and 17.6% for SHA/5Al_2O_3 after sintering at 1300°C was calculated. However; in the SHA/10Al_2O_3 composite, 19.2% of HA transformed into β-TCP and 1.0% of HA to α-TCP, after sintering was carried out at 1100°C. When it was sintered at 1300°C, the transformation rate of HA into β-TCP and α-TCP increased to 43.4% and 16.7%, respectively. In addition to β- and/ α-TCP, calcium aluminates ($CaAl_2O_4$ and $Ca_4Al_6O_{13}$) were detected in the SHA/Al_2O_3 composites. No CaO peak was observed in the SHA/Al_2O_3 composites. CaO in free form has observed in HA/ZrO_2 [53] and HA/TiO_2 [54] composites.

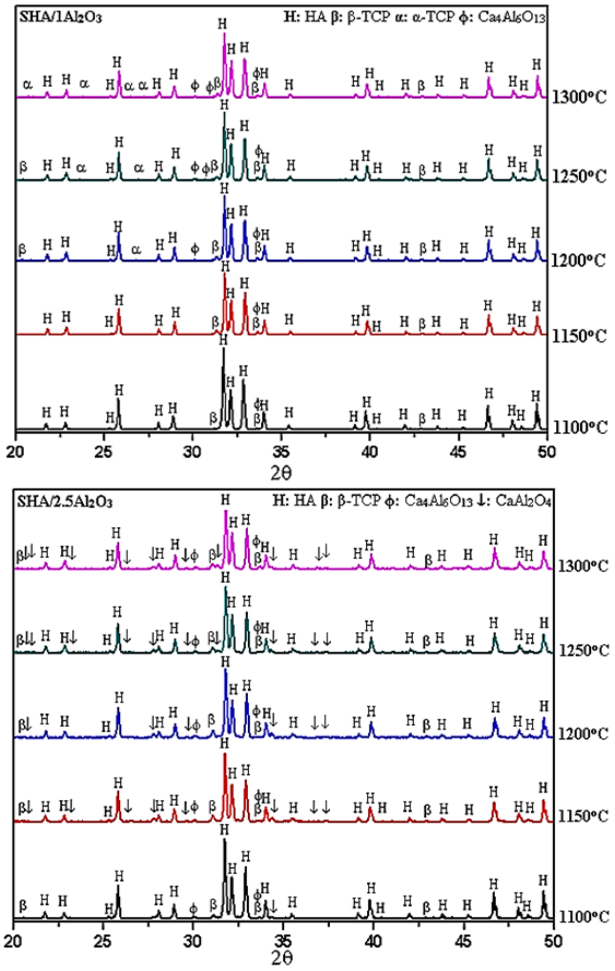

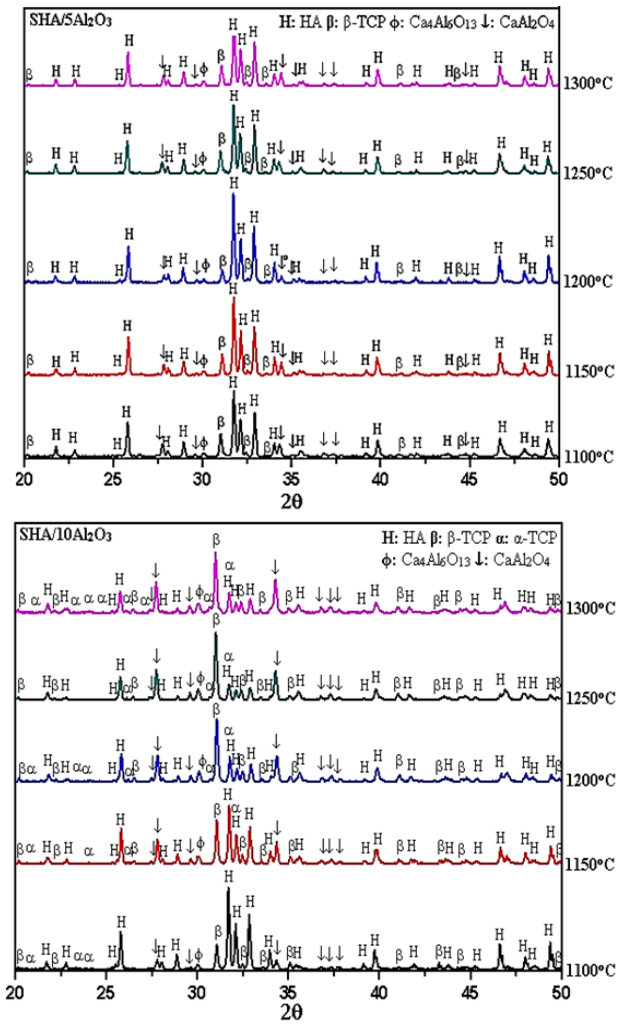

Figure 4. XRD patterns of Al_2O_3 added SHAs

Table 2. Rietveld analysis of SHA-Al_2O_3 composites depending on the sintering temperatures

Temperature (°C)	Composite	Chemical composition (%)					Total decomposition ratio (%)
		HA	β-TCP	α-TCP	$Ca_4Al_6O_{13}$	$CaAl_2O_4$	
1100	SHA-1Al_2O_3	94.1	2.8	-	3.1	-	2.8
1150		92.9	3.2	-	3.9	-	3.2
1200		90.5	3.7	1.7	4.1	-	5.4
1250		88.7	4.1	2.4	4.8	-	6.5
1300		87.0	5.0	3.0	5.0	-	8.0
1100	SHA-2.5Al_2O_3	92.9	3.1	-	3.8	0.2	3.1
1150		91.1	4.5	-	4.0	0.4	4.5
1200		90.3	5.0	-	4.2	0.5	5.0
1250		87.0	6.6	-	5.0	1.4	6.6
1300		84.8	8.1	-	5.4	1.7	8.1
1100	SHA-5Al_2O_3	90.4	4.8	-	3.2	1.6	4.8
1150		89.4	5.2	-	3.5	1.9	5.2
1200		85.6	7.5	-	4.9	4.0	7.5
1250		79.1	13.7	-	4.2	5.0	13.7
1300		74.5	17.6	-	3.8	8.9	17.6
1100	SHA-10Al_2O_3	71.6	19.2	1.0	1.2	7.0	20.2
1150		62.5	25.8	2.9	1.4	7.4	28.7
1200		55.9	30.4	4.2	1.5	8.0	34.6
1250		43.8	37.6	8.5	1.6	8.5	46.1
1300		25.6	43.4	16.7	2.0	12.3	60.1

Figure 5 (a-c) shows the density, porosity and relative density of SHA and SHA/Al_2O_3 composites depending on the sintering temperatures, respectively. The density of pure SHA calculated as 2.16±0.03 g/cm^3 at 1100°C increased with increasing temperature and reached

2.98±0.02 g/cm^3 at 1300ºC. However, the highest densities in Al_2O_3 added SHAs could be obtained at different temperatures depending on the amount of Al_2O_3 additives. The highest density in composites was calculated as 2.95±0.00 g/cm^3, and it belongs to SHA-1Al_2O_3. In general, a decrease in the densities of the composites was determined with the increase of the Al_2O_3 ratio. Similar behavior had also confirmed in Al_2O_3 added bovine HA [55] and synthetic HA [56]. The relative density of SHA at 1100ºC calculated as 68.58±0.74% increased to 94.48±0.64% when sintering temperature is 1300ºC. A maximum relative density value of 94.29±0.12% could be achieved in Al_2O_3 added SHAs and it belongs to SHA-2.5Al_2O_3 composite sintered at 1200ºC. However, the relative density of this composite decreased to 90.96±0.54% with increasing temperature. A similar situation has been observed in SHA-5Al_2O_3 composites, and its relative density decreased from %89.49±1.10 to %82.61±1.71 with the temperature increasing from 1200ºC to 1300ºC. The highest relative densities for SHA-1Al_2O_3 and SHA-10Al_2O_3 composites could be obtained at 1250ºC, and they were calculated as 93.65±0.14% and 82.08±0.96%, respectively. As can be seen from these values, the density and partial density of Al_2O_3 added SHAs are affected by several factors. First, the increased Al_2O_3 ratio caused the decomposition rate of HA to increase from 2.8% to 60.1%, as seen in Table 2. The increase in the decomposition ratio resulted in the formation of β-TCP (3.07 g/cm^3 [57]), and α-TCP (2.866 g/cm3 [58]) phases, which have lower theoretical density values than that of HA (3.156 g/cm^3). Secondly, increasing Al_2O_3 ratio increases the formation of $CaAl_2O_4$ phase, which is one of the two detected calcium aluminate phases in SHA-Al_2O_3 composites. Because $CaAl_2O_4$ (2.98 g/cm^3 [59]) has a lower theoretical density than HA, just like β-TCP and α-TCP phases, the densification behavior of the composites has decreased. Moreover, it has an increasing effect on the decomposition of HA in HA-Al_2O_3 binary composites as seen in Reaction 2 [60].

$$Ca_{10}(PO_4)_6(OH)_2 + Al_2O_3 \longrightarrow 3Ca_3(PO_4)_2 + CaAl_2O_4 + H_2O \quad \text{(R.2)}$$

SHA-1Al_2O_3 and SHA-2.5Al_2O_3 composites have higher densification behavior than SHA-5Al_2O_3 and SHA-10Al_2O_3 composites because these composites contain higher amount of $Ca_4Al_6O_{13}$ as shown in Table 2. $Ca_4Al_6O_{13}$ has a higher theoretical density (3.548 g/cm^3 [61]) than $CaAl_2O_4$. The increase in $CaAl_2O_4$ ratio increases the release of OH^- ions and causes a more porous structure [62]. Therefore, SHA-5Al_2O_3 and SHA-10Al_2O_3 composites are more porous than SHA-1Al_2O_3 and SHA-2.5Al_2O_3. The lowest porosity in SHA-5Al_2O_3 and SHA-10Al_2O_3 composites were calculated as 7.20±0.37%, and 11.15±1.19%, respectively. It was calculated as 2.45±0.60% for SHA-1Al_2O_3, and 2.53±0.42% for SHA-2.5Al_2O_3 composites.

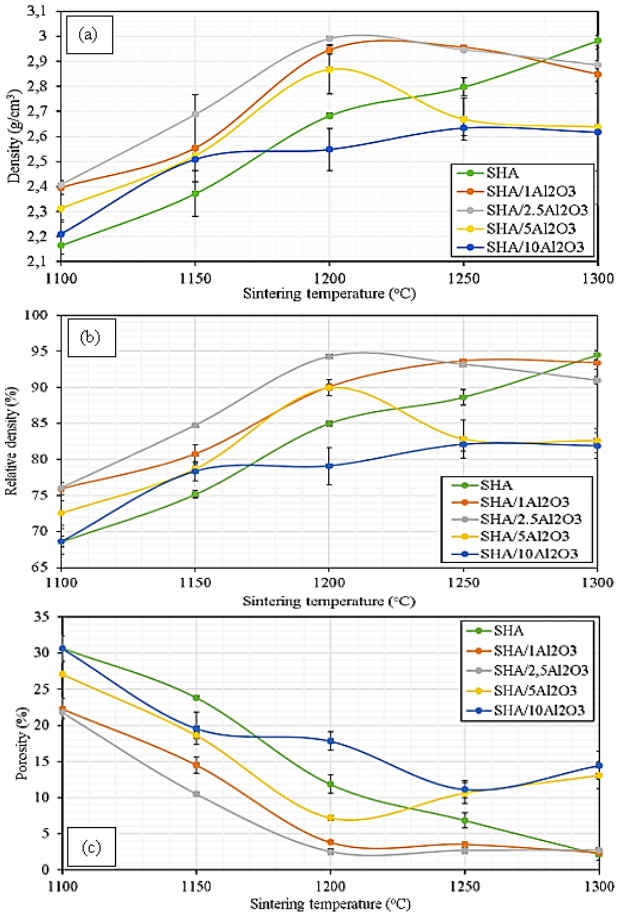

Figure 5. (a) Density, **(b)** porosity, and **(c)** relative density of SHA and SHA/Al_2O_3 composites depending on the sintering temperatures

Figure 6 shows the compression strength of SHA and SHA-Al_2O_3 composites. The compression strength of SHA calculated as 35.14±2.51 MPa at 1100ºC increased to 82.48±5.50 MPa at 1200ºC, but decreased to 73.55±4.04 and 64.27±3.05 MPa when sintering was carried out 1250 and 1300ºC. There are two reasons why the compression strength of SHA decreases at temperatures above 1200ºC: First is the decomposition of SHA into α-TCP and CaO phases, which have lower compression strength than β-TCP, as shown in **Table 3**. Second is the average grain size of 1.404 at 1200ºC showed a great deal with increasing temperature, and reached to 3.632±0.716 µ, as shown in Figure 7.

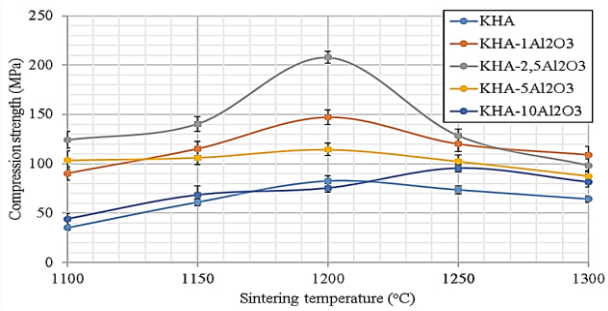

Figure 6. Compression strength of SHA and SHA-Al_2O_3 composites.

Table 3. The mechanical properties of β-TCP, α-TCP and CaO

Property	β-TCP	α-TCP	CaO
Compression strength (MPa)	436 [63]	42 [64]	38.6 [65]

In line with previously reported study, it has been observed that with increase in grain size such as from 1.3 µ to 3.5 µ [66], compression strength of HA decrease.

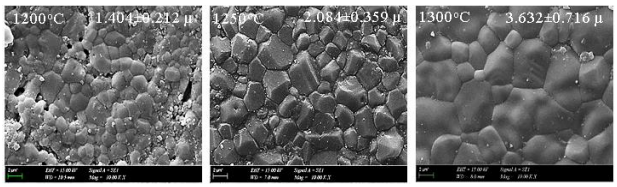

Figure 7. SEM images of SHA sintered at 1200ºC, 1250ºC and 1300ºC.

Figure 8 shows the SEM images of SHA-1Al_2O_3 and SHA-2.5Al_2O_3 composites sintered between 1200 and 1300ºC. It was determined that with the addition of 2.5% Al_2O_3 to SHA, the grain growth in SHA could be prevented at a higher rate than %1Al_2O_3. This can be attributed to the $Ca_4Al_6O_{13}$. As seen in Reaction 3, the $Ca_4Al_6O_{13}$ phase occurs in HA-Al_2O_3 composites from 900ºC to 1300ºC [59] and it has an inhibitory effect on grain growth.

$$4CaO + 3Al_2O_3 \longrightarrow Ca_4Al_6O_{13} \qquad (R.3)$$

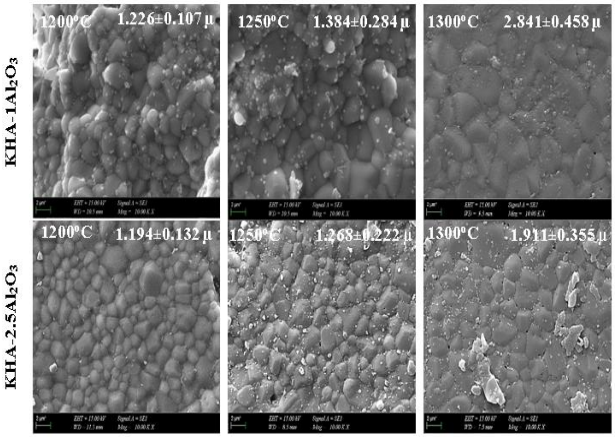

Figure 8. SEM images of SHA-1Al_2O_3 and SHA-2.5Al_2O_3 composites

For HA compacts mechanical properties are enhanced with decrease in grain size in sintered microstructure. With decrease in grain size, the inherent flaw size in sintered microstructure is reduced which leads to the enhancement of compressive strength. Again as the number of grain boundaries per unit volume is increased with decrease in grain size, finer grain sized compacts offer more resistance to crack propagation and dislocation motion resulting in higher hardness and fracture toughness [67]. The highest compression strength of SHA of 82.48±5.50 MPa could be increased to 147.29±7.50 MPa, 207.85±5.85 MPa, 114.50±6.16 MPa and 95.45±3.53 MPa by increase in Al_2O_3 ratio in the present study. The highest compression strength belongs to SHA-2.5Al_2O_3 composite and it is about 2.5 times higher than Bovine HA-Al_2O_3 composite [55]. Figure 9 a-c show the hardness, fracture tougness and brittleness index of SHA with and without Al_2O_3 additives. The hardness of SHA at 1100ºC calculated as 0.93±0.15 GPa increased to the highest value of 3.90±0.27 GPa when sintering was performed at 1300ºC. However, the highest fracture toughness for SHA was obtained by sintering at 1200ºC and it was calculated as 0.70±0.11 $MPam^{1/2}$. The highest fracture toughness values were obtained at 1200ºC in Al_2O_3 added SHAs and they were calculated as 1.32±0.06, 1.70±0.15, 1.41±0.27 and 1.11±0.24 $MPam^{1/2}$ depending on the increasing Al_2O_3 ratio. As can be seen from these values, an increase in the fracture toughness of SHA between 1.5 and 2.5 times was achieved with the addition of Al_2O_3. There are several reasons for this: First is the Al_2O_3 (3.72 $MPam^{1/2}$ [68]) used as reinforcement material has higher fracture toughness than HA. Second, the calcium aluminate phases formed between HA and Al_2O_3 particles limit the propagation of post-indentation cracks [69]. Third is because the ratio of β-TCP in the composites is higher than that of pure SHA, the fracture toughness of β-TCP (1.28 $MPam^{1/2}$ [70]) is approximately 80% higher than HA, contributing to the increase in fracture toughness. The brittleness index of SHA without Al_2O_3 increased from 1.70±0.27 to 7.10±0.50 $\mu^{-1/2}$ with increasing temperature. The brittleness index of SHA at 1200ºC, where the highest fracture toughness and compressive strength is obtained, is 4.26±0.50 $\mu^{-1/2}$, and it is compatible with 4.85 found by Shaly et al. [71].

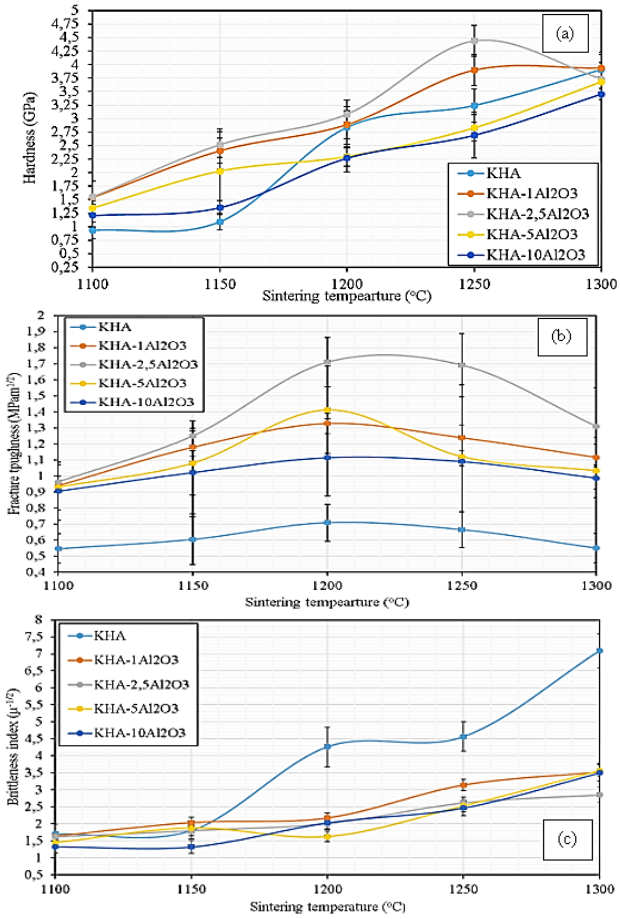

Figure 9. (a) Hardness, (b) fracture toughness, and (c) brittleness index of SHA with and without Al_2O_3 additives

The brittleness index of SHA-Al_2O_3 composites increased with increasing temperature, just as in pure SHA. However, it increased to 3.56±0.18 $\mu^{-1/2}$ as the maximum value. As can be seen from this value, the maximum brittleness index of SHA was reduced by about 1/2. It is also compatible with MgO added synthetic HA calculated as 3.72 $\mu^{-1/2}$ [72].

Figure 10 shows the SEM and EDS analysis of pure SHA and SHA-2.5Al_2O_3 composite subjected to SBF testing during immersion periods of 14 and 28 days, respectively. At the end of the 14 days immersion, the apatite layer with a Ca/P ratio of 1.77 was crystallized on the SHA surface. After 28 days, the Ca/P ratio decreased to 1.76 and most of the SHA surface was covered with apatite layer. However, the surface of SHA-2.5Al_2O_3 composite was mostly covered with apatite layer in both 14 and 28-day immersion times. While the Ca/P ratio of the apatite layer formed on the surface of the SHA-2.5Al_2O_3 composite after 14 days was 1.87, it was calculated as 1.69 at the end of 28 days. It has a Ca/P ratio closer to the ideal value of 1.67 [73]. It has been concluded that there may be several reasons why SHA with 2.5% Al_2O_3 addition exhibits better bioactivity than pure SHA. As stated by Sainz et al., average grain size and phases contained in the samples subjected to the SBF test affect the precipitation of apatite layers [74]. The smaller the average grain size, the higher the apatite layer precipitation on the surface of the samples subjected to the SBF testing [75]. The average grain sizes of SHA and SHA-2.5Al_2O_3 subjected to the SBF test in this study are 1.404±0.212 µ and 1.194±0.132 µ. As mentioned earlier, there are two phases that contribute to the formation of a lower grain size in the SHA-Al_2O_3 composite than in SHA: $Ca_4Al_6O_{13}$. As noted by García-Álvarez et al. [76] that $CaAl_2O_4$ exhibits a triggering effect on the apatite precipitation from the SBF solution.

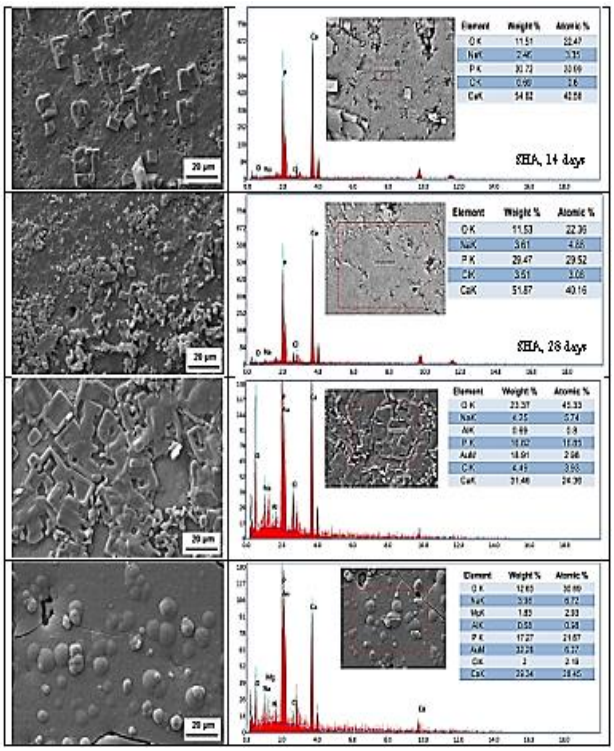

Figure 10. SEM and EDS analysis of pure SHA and SHA-2.5Al_2O_3 composite subjected to SBF testing during immersion periods of 14 and 28 days

4. CONCLUSIONS

In this study, the effects of Al_2O_3 addition at 4 different rates on the properties of SHA were examined and the following results were obtained:

1- SHA decomposed into β-TCP between 1100ºC-1200ºC, β- and α-TCP at 1250ºC and β- and α-TCP + CaO phases at 1300ºC, and the decomposition rate increased from 1.4% to 4.1% with increasing sintering temperature.
2- With increasing Al_2O_3 and sintering temperature, 60.1% of HA in the SHA-Al_2O_3 composites decomposed into β- and α-TCP phases.
3- Density, hardness and brittleness index properties of SHA without Al_2O_3 additive increased with increasing temperature, however; the highest compression strength and fracture toughness were obtained at 1200ºC.
4- With the addition of Al_2O_3 at amount of 2.5%, the highest fracture toughness and compression strength values of SHA were increased approximately 2.5 times.
5- The amount of apatite layer formed on the surface of SHA-2.5Al_2O_3 composite is higher than SHA due to its lower grain size and the phases it contains.

REFERENCES

[1] Boutinguiza M., Pou J., Comesaña R., Lusquiños F., de Carlos A., León B. Biological hydroxyapatite obtained from fish bones. Mater. Sci. Eng. C. 2012;32:478-86.
[2] Hart A., Ebiundu K., Peretomode E., Onyeaka H., Nwabore O.F., Obileke K. Value-added materials recovered from waste bone biomass: technologies and applications. RSC Adv. 2022;12:22302-20.
[3] Buddhachat K., Klinhom S., Siengdee P., Brown J.L., Nomsiri R., Kaewmong P., Thitaram C., Mahakkanukrauh P., Nganvongpanit K. Elemental analysis of bone, teeth, horn and antler in different animal species using nonınvasive handheld X-ray fluorescence. PloS One. 2016; doi: 10.1371/journal.pone.0155458.
[4] Hussain F., Alshahrani S., Abbas M.M., Khan H.M., Jamil A., Yaqoob H., Soudagar M., Imran M., Ahmad M., Munir M. Waste animal bones as catalysts for biodiesel production; A mini review. Catalysts. 2021;11:630-45.
[5] Foroutan R., Peighambardoust S.J., Hosseini S.S., Akbari A., Ramavandi B. Hydroxyapatite biomaterial production from chicken (femur and beak) and fish bone waste through a chemical less method for Cd^{2+} removal from shipbuilding waste water. J. Hazard. Mater. 2021;413:125428-40.
[6] Esmaeilkhanian A., Sharifianjazi F., Abouchenari A., Rouhani A., Parvin N., Irani M. Synthesis and characterization of natural nano-hydroxyapatite derived from turkey femur-bone waste. Appl. Biochem. Biotechnol. 2019;189:919-32.
[7] Herliansyah M.K., Dewo P., M. Shukor H.A., Ide-Ektessabi Ari. Development and characterization of bovine hydroxyapatite porous bone graft for biomedical applications. Adv. Mater. Res. 2011;277:59-65.
[8] Ismail S.A., Abdullah H.Z. Extraction and characterization of natural hydroxyapatite from goat bone for biomedical applications. Mater. Sci. Forum. 2020;1010:573-78.

[9] Buasri A., Inkaew T., Kodephun L., Yenying W., Loryuenyong V. Natural hydroxyapatite (NHAp) derived from pork bone as a renewable catalyst for biodiesel production via microwave irradiation. Key Eng. Mater. 2015;659:216-20.
[10] Sartoretto S.C., Uzeda M.J., Miguel F.B., Nascimento J.R., Ascoli F., Calasans-Maia M.D. Sheep as an experimental model for biomaterial implant evaluation. Acta Ortop Bras. 2016;24(5):262-66.
[11] Li Y., Chen S.K., Li L., Qin L., Wang X.L., Lai Y.X. Bone defect animal models for testing efficacy of bone substitute biomaterials. J. Orthop. Translat. 2015;3:95-04.
[12] Rehman I., Smith R., Hench L.L., Bonfield W. Structural evaluation of human and sheep, bone and comparison with synthetic hydroxyapatite by FT-Raman spectroscopy. J. Biomed. Mater. Res. 1995;29(10):1287-94.
[13] Indra A., Putra A.B., Handra N., Fahmi H., Nurzal A., Perdana M., Subardi A., Jon Affi J. Behavior of sintered body properties of hydroxyapatite ceramics: effect of uniaxial pressure on green body fabrication. Mater. Today Sustain. 2022;17:100100-08.
[14] Demirkol N., Oktar F.N., Kayali E.S. Influence of niobium oxide on the mechanical properties of hydroxyapatite. Key Eng. Mater. 2013;529-530: 29-33.
[15] Angioni D., Cannillo V., Orrù R., Cao G., Garroni S., Bellucci D. Bioactivity enhancement by a ball milling treatment in novel bioactive glass-hydroxyapatite composites produced by spark plasma sintering. J. Eur. Ceram. Soc. 2023;43:1220-29.
[16] Bazin T., Magnaudeix A., Mayet R., Carles P., Julien I., Demourgues A., Gaudon M., Champion E. Sintering and biocompatibility of copper-doped hydroxyapatite bioceramics. Ceram. Int. 2021;47:13644-54.
[17] Demirkol N., Oktar F.N., Kayali E.S. Mechanical and microstructural properties of sheep hydroxyapatite (SHA)-niobium oxide composites. Acta Phys. Pol. A. 2012;121(1):274-76.
[18] Akıllı A., Evlen H., Demirkol N. Biological and morphological effects of apatite kinds (Sheep/Synthetic) on MgO reinforced bone tissue with hydroxyapatite matrix. Acta Phys. Pol. A. 2022;142(2):201-10.
[19] Karip E., Muratoğlu M. A study on using expanded perlite with hydroxyapatite: Reinforced bio-composites. Proc. Inst. Mech. Eng. H: J. Eng. Med. 2021;235(5):574-82.
[20] Ekren N. Reinforcement of sheep-bone derived hydroxyapatite with bioactive glass. J. Ceram. Process. Res. 2017;18(1):64-68.
[21] Landek D., Ćurković L., Gabelica I., Mustafa M.K., Žmak I. Optimization of sintering process of alumina ceramics using response surface methodology. Sustainability. 2021;13:6739-53.
[22] Pan Y., Li H., Liu Y., Liu Y., Hu K., Wang N., Lu Z., Liang J. He S. Effect of holding time during sintering on microstructure and properties of 3D printed alumina ceramics. Front. Mater. 2020;7:54-66.
[23] Zhang L., Liu H., Yao H., Zeng Y., Chen J. Preparation, microstructure, and properties of ZrO_2(3Y)/Al_2O_3 bioceramics for 3D printing of all-ceramic dental implants by vat photopolymerization. Chin. J. Mech. Eng. 2022;1(2):100023-36.
[24] Visbal S., Lira-Olivares J., Sekino T., Niihara K., Moon B.K., Lee S.W. Mechanical properties of Al_2O_3-TiO_2-SiC nanocomposites for the femoral head of hip joint replacement. Mater. Sci. Forum. 2005;486-487:197-00.
[25] Aminzare M., Eskandari A., Baroonian M.H., Berenov A., Hesabi Z.R., Taheri M., Sadrnezhaad S.K. Hydroxyapatite nanocomposites: Synthesis, sintering and mechanical properties. Ceram. Int. 2013;39:2197-06.
[26] Epure L.M., Dimitrievska S., Merhi Y., Yahia L.H. The effect of varying Al_2O_3 percentage in hydroxyapatite/Al_2O_3 composite materials: Morphological, chemical and cytotoxic evaluation. J. Biomed. Mater. Res. 2007;83A(4):1009-23.
[27] Ji H., Marquis P.M. Preparation and characterization of Al_2O_3 reinforced hydroxyapatite. Biomaterials. 1992;13(11):744-48.
[28] Öksüz K.E., Özer A. Microstructural and phase study of Y_2O_3 doped hydroxyapatite/Al_2O_3 biocomposites. Dig. J. Nanomater. Biostructures. 2016;11(1):167-72.
[29] Mezahi F.Z. Effect of ZrO_2, TiO_2, and Al_2O_3 additions on process and kinetics of bonelike apatite formation on sintered natural hydroxyapatite surfaces. Int. J. Appl. Ceram. Technol. 2012;9(3):529-40.
[30] British Standard Non-Metallic Materials for Surgical Implants. Part 2: Specifications for Ceramic Materials Based on Alumina, BS 7253: Part 2: 1990 ISO 6474-1981.
[31] Majling J., Znáik P., Palová A., Stevĭk S., Kovalĭk S., Agrawal D.K., Roy R. Sintering of the ultrahigh pressure densified hydroxyapatite monolithic xerogels. J. Mater. Res. 1997;12(1):198-02.
[32] Rahimiana M., Ehsani N., Parvin N., Baharvandi H.R. The effect of particle size, sintering temperature and sintering time on the properties of Al-Al_2O_3 composites, made by powder metallurgy. J. Mater. Process. Technol. 2009;209:5387-93.
[33] Niihara K. Indentation microfracture of ceramics-its application and problems. J. Ceram. Soc. Jpn. 1985;20:12-18.
[34] Pandey A., Nigam V.K., Balani K. Multi-length scale tribology of hydroxyapatite reinforced with ceria and silver. Wear. 2018;404-405:12-21.
[35] Demirkol N., Turan M. Production and characterization of ternary sheep hydroxyapatite (SHA)-wollastonite (W)-commercial inert glass (CIG) biocomposite. Res. Eng. Struct. Mater. 2019;5(2):167-74.
[36] Kim S.R., Lee J.H., Kim Y.T., Riu D.H., Jung S.J., Lee Y.J., Chung S.C., Kim Y.H. Synthesis of Si, Mg substituted hydroxyapatites and their sintering behaviors. Biomaterials. 2003;24:1389-99.

[37] Herliansyah M.K., Hamdi M., Ide-Ektessabi A., Wildan M.W., Toque J.A. The influence of sintering temperature on the properties of compacted bovine hydroxyapatite. Mater. Sci. Eng. C 2009;29:1674-80.
[38] Liao C.J., Lin F.H., Chen K.S., Sun J.S. Thermal decomposition and reconstitution of hydroxyapatite in air atmosphere. Biomaterials. 1999;20:1807-13.
[39] Rapacz-Kmita A., Paluszkiewicz C., Ślósarczyk A., Paszkiewicz Z. FTIR and XRD investigations on the thermal stability of hydroxyapatite during hot pressing and pressureless sintering processes. J. Mol. Struct. 2005;744-747:653-56.
[40] Göller G., Oktar F.N. Sintering effects on mechanical properties of biologically derived dentine hydroxyapatite. Mater. Lett. 2002;56:142-47.
[41] Niakan A., Ramesh S., Tan C.Y., Hamdi M., Teng W.D. Characteristics of sintered bovine hydroxyapatite. Appl. Mech. Mater. 2013;372:177-80.
[42] Rao R.R., Kannan T.S. Synthesis and sintering of hydroxyapatite–zirconia composites. Mater. Sci. Eng. C 2002;20:187-93.
[43] Indrani D.J., Soegijono B., Adi W.A., Trout N. Phase composition and crystallinity of hydroxyapatite with various heat treatment temperatures. Int. J. App. Pharm. 2017;9(2):87-91.
[44] Wei L., Pang D., He L., Deng C. Crystal structure analysis of selenium-doped hydroxyapatite samples and their thermal stability. Ceram. Int. 2017;43:16141-48.
[45] Xu J.L., Khor K.A. Chemical analysis of silica doped hydroxyapatite biomaterials consolidated by a spark plasma sintering method. J. Inorg. Biochem. 2007;101:187-95.
[46] Lim K.F., Muchtar A., Mustaffa R., Tan C.Y. Sintering of HA/Zirconia composite for biomedical and dental applications: A review. Adv. Mater. Res. 2013;686:290-95.
[47] The British Standards Institution 2018, ISBN 978 0 580 86939-6
[48] Santos J.D., Silva P. L., Knowles J. C., Talal S., Monteiro F. J. Reinforcement of hydroxyapatite by adding P_2O_5-CaO glasses with Na_2O, K_2O and MgO. J. Mater. Sci.: Mater. Med. 1996;7:187-89.
[49] Sung Y.M., Lee J.C., Yang J.W. Crystallization and sintering characteristics of chemically precipitated hydroxyapatite nanopowder. J. Cryst. Growth. 2004;262:467-72.
[50] Ou S.F., Chiou S.Y., Ou K.L. Phase transformation on hydroxyapatite decomposition. Ceram. Int. 2013;39:3809-16.
[51] Youness R.A., Taha M.A., Ibrahim M.A. Effect of sintering temperatures on the in vitro bioactivity, molecular structure and mechanical properties of titanium/carbonated hydroxyapatite nano biocomposites. J. Mol. Struct. 2017;1150:188-95.
[52] Sobczak-Kupiec A., Wzorek Z. The influence of calcination parameters on free calcium oxide content in natural hydroxyapatite. Ceram. Int. 2012;38:641-47.
[53] Evis Z., Usta M., Kutbay I. Improvement in sinterability and phase stability of hydroxyapatite and partially stabilized zirconia composites. J. Eur. Ceram. Soc. 2009;29:621-28.
[54] Nath S., Tripathi R., Basu B. Understanding phase stability, microstructure development and biocompatibility in calcium phosphate-titania composites, synthesized from hydroxyapatite and titanium powder mix. Mater. Sci. Eng. C 2009;29(1):97-07.
[55] Oktar F.N., Agathopoulos S., Ozyegin L.S., Gunduz O., Demirkol N., Bozkurt Y., Salman S. Mechanical properties of bovine hydroxyapatite (BHA) composites doped with SiO_2, MgO, Al_2O_3, and ZrO_2. J. Mater. Sci: Mater. Med. 2007;18:2137-43.
[56] Tayyebi S., Mirjalili F., Samadi H., Nemati A. A review of synthesis and properties of hydroxyapatite/alumina nano composite powder. J. Chem. 2015;5(2):20-28.
[57] Bohner M., Santoni B.L.G., Döbelin N. β-tricalcium phosphate for bone substitution: Synthesis and properties. Acta Biomater. 2000;13:23-41.
[58] Sinusaite L., Renner A.M., Schütz M.B., Antuzevics A., Rogulis U., Grigoraviciute-Puroniene I., Mathur S., Zarkov A. Effect of Mn doping on the low-temperature synthesis of tricalcium phosphate (TCP) polymorphs. J. Eur. Ceram. Soc. 2019;39(10):3257-63.
[59] Kahlenberg V., Fischer R.X., Shaw C.S.J. High-pressure Ca_4Al_6O13: An example of a calcium aluminate with three different types of coordination polyhedra for aluminum. Am. Mineral. 2000;85:1492-96.
[60] Kumar P.N., Ferreira J.M.F., Kannan S. Phase transition mechanisms involved in the formation of structurally stable β-$Ca_3(PO_4)_2$-α-Al_2O_3 composites. J. Eur. Ceram. Soc. 2017;37:2953-63.
[61] Mei H., Zhong Y., Wang P., Jia Z., Li C., Cheng N. Electronic, optical, and lattice dynamical properties of tetracalcium trialuminate ($Ca_4Al_6O_{13}$). Materi. 2018;11:449-61.
[62] Salomão R., Ferreira V.L., Costa L.M.M., de Oliveira I.R. Effects of the initial CaO-Al_2O_3 ratio on the microstructure development and mechanical properties of porous calcium hexaluminate. Ceram. Int. 2017;42(2):2626-31.
[63] Akao M., Aoki H., Kato K., Sato A. Dense polycrystalline β-tricalcium phosphate for prosthetic applications. J. Mater. Sci. 1982;17:343-46.
[64] Takahashi K., Fujishiro Y., Yin S., Sato T. Preparation and compressive strength of a-tricalcium phosphate based cement dispersed with ceramic particles. Ceram. Int. 2004;30:199-03.
[65] Mimi M. M., Shakil A.-M.-O.-R., Haque M. R., Hasan, M. R. Effect of addition of CaO on compressive strength of high-volume fly ash concrete. J. Civ. Eng. Sci. Technol. 2003;14(1):64-76.
[66] Trzaskowska M., Vivcharenko V., Przekora A. The impact of hydroxyapatite sintering temperature on its microstructural, mechanical, and biological properties. Int. J. Mol. Sci. 2023;24:5083-04.

[67] Dasgupta S., Tarafder S., Bandyopadhyay A., Bose S. Effect of grain size on mechanical, surface and biological properties of microwave sintered hydroxyapatite. Mater. Sci. Eng. C 20123;33:2846-54.
[68] Szutkowska M. Fracture toughness of advanced alumina ceramics and alumina matrix composites used for cutting tool edges. J. Achiev. Mater. Manuf. Eng. 2012;54(2):202-10.
[69] Afzal M.A.F., Kesarwani P., Reddy K.M., Kalmodia S., Basu B., Balani K. Functionally graded hydroxyapatite-alumina-zirconia biocomposite: Synergy of toughness and biocompatibility. Mater. Sci. Eng. C 2012;32:1164-73.
[70] Akao M., Miura N., Aoki H. Fracture toughness of sintered hydroxyapatite and β-tricalcium phosphate. JCS-Japan. 1984;92(107):672-74.
[71] Shaly A.A., Priya G.H., Mahendiran M., Linet J.M., Arul J., Mani M. An intrinsic analysis on the nature of alumina (Al_2O_3) reinforced hydroxyapatite nanocomposite. Physica B: Condensed Matter. 2022;642(1):414100.
[72] Shaly, A.A., Priya, G.H., Linet, J.M.: An exploration on the configurational and mechanical aspects of hydrothermally procured MgO/HA bioceramic nanocomposite. Phys. B 2021;617:413131
[73] Chien C.S., Liao T.Y., Hong T.F., Kuo T.Y., Chang C.H., Yeh M.L., Lee T.M. Surface microstructure and bioactivity of hydroxyapatite and fluorapatite coatings deposited on Ti-6Al-4V substrates using Nd-YAG laser. J. Med. Biol. Eng. 2014; 34(2):109-15.
[74] Sainz M.A., Pena P., Serena S., Caballero A. Influence of design on bioactivity of novel $CaSiO_3$-$CaMg(SiO_3)_2$ bioceramics: In vitro simulated body fluid test and thermodynamic simulation. Acta Biomater. 2010;6:2797-07.
[75] Wu C., Chang J. Synthesis and in vitro bioactivity of bredigite powders. J. Biomater. Appl. 2007;21: 251-63.
[76] García-Álvarez J., Escobedo-Bocardo C., Cortés-Hernández D.A., Almanza-Robles J. M. Bioactivity and mechanical properties of scaffolds based on calcium aluminate and bioactive glass. Int. J. Mater. Res. 2018;110(4):343-50.